Critical Tube Diameter for Quasi-Detonations

Xuxu Sun[a,b], Chian Yan[c], Yiran Yan[d], Xiaocheng Mi[d,e], John H.S. Lee[d], Hoi Dick Ng[c]

[a]*School of Safety Science and Emergency Management,Wuhan University of Technology, Wuhan, 430081, China*
[b]*State Key Laboratory of Fire Science, University of Science and Technology of China, Hefei, 230027, China*
[c]*Department of Mechanical, Industrial and Aerospace Engineering, Concordia University, Montreal, H3G 1M8, QC, Canada*
[d]*Department of Mechanical Engineering, McGill University, Montreal, H3A 2K6, QC, Canada*
[e]*Department of Mechanical Engineering, Eindhoven University of Technology, Eindhoven, 5600 MB, the Netherlands*

Abstract

The critical tube diameter problem for quasi-detonations is studied via experiments and two-dimensional numerical simulations based on the reactive Euler equations. In the experiments, quasi-detonation in stoichiometric acetylene-oxygen mixtures is generated in rough-walled tubes with three different diameters, where the wall roughness is introduced by using spiral inserts with different wire diameters. Photodiodes are placed along the rough tubes to record the detonation time-of-arrival to deduce the velocity, and a high-speed schlieren system is used to observe the diffraction processes. Near the critical regime of detonation diffraction, the quasi-detonation emerging from the rough tube is again shown to first fail and subsequently re-initiate from a local explosion center in the spherical deflagration reaction zone. For quasi-detonations, stronger turbulence and instabilities produce stronger local hot spots, which balances the significant velocity deficit as much as approximately 15% in the rough tube, resulting in the critical pressure remaining relative constant. The cell sizes for quasi-detonation in rough tubes are directly measured, and the ratio of critical tube diameters (d_c) to these determined cell sizes (λ) is used to quantify the critical criterion of detonation

Email address: hoing@encs.concordia.ca (Hoi Dick Ng)

initiation. In rough tubes with coil springs, the previous criterion of $d_c/\lambda \geqq 13$ for detonation re-initiation appears invalid, and the critical initiation regime for quasi-detonation in rough tubes is found approximately as $d_c/\lambda \geqq 8$. Despite the cell enlargement and the lower propagation velocity for quasi-detonation, it is hypothesized that the increase in cell irregularities or instabilities can in turn benefit the transmission process. These unstable features of quasi-detonation are supported by the two-dimensional numerical simulations, also showing a higher degree of cell irregularities, a wider spectrum of induction rate, and the generation of shocked reactive pockets.

Keywords: Detonation, supersonic combustion, detonation limit, critical tube diameter, quasi-detonation, rough wall, d_c/λ

---

1. Introduction

Critical tube diameter for detonation transmission

Critical tube diameter for detonation transmission, d_c, refers to the minimum diameter of a tube from which an exiting detonation can successfully evolve into a spherical detonation in an unconfined space. Quenching of the incident detonation can be observed emerging from tube diameters smaller than d_c. This critical phenomenon of gaseous detonations was first observed by Zel'dovich *et al.* [1] and later studied by Mitrofanov and Soloukhin [2]. Besides its significance in reflecting the fundamental mechanisms of detonation propagation and failure [3, 4], critical tube diameter is an essential piece of information for developing real-world applications of gaseous detonation, e.g., in pulsed and rotating detonation engines where a detonation transmits from small pre-detonator tubes into the main thrust chamber [5, 6]. Hence, there is a renewed interest in re-visiting this fundamental problem, both computationally and experimentally, with more advanced computational techniques and flow diagnostics.

The most pioneering efforts on the critical-tube-diameter problem of gaseous detonations were summarized by Lee [3, 7]. An important finding of these studies is that the experimentally determined d_c correlates with the intrinsic detonation cell size, λ. For detonations characterized by an irregular cellular structure, typically, in undiluted mixtures of hydrocarbon fuels and oxygen [8–11], the universal correlation of $d_c/\lambda \approx 13$ has been identified. In contrast, for weakly unstable detonations, featuring a regularly spaced cellular pattern, e.g., in highly diluted mixtures, the critical diameter scaling can

be as large as $d_c/\lambda \approx$ 20-30 [12–14]. This significant difference in d_c/λ scaling between highly and weakly unstable detonations suggests that the cellular instabilities play an important role in the critical phenomenon of detonation re-initiation and failure. More recently, the experimental investigations by Nagura *et al.* [15] and subsequently Kawasaki Kasahara [16] proposed a new length for scaling relevant to the process of supercritical diffraction based on the reflection point distance (i.e., distance from the channel end corner to the reflection point of the transverse detonation on the channel end face), regardless the mixture is unstable or stable.

Many investigations have been performed by different researchers on the fundamental detonation diffraction problem with more advanced computational techniques, analytical concepts and experimental flow diagnostics. Using Eckett *et al.* model [17], Pintgen and Shepherd [18] described detonation diffraction from the effect of unsteadiness in the reaction process and obtained the critical condition by linking it to the decay rate of the wave front velocity, which is a function of the effective mixture activation energy dictating the change in induction time for changes in the lead shock strength. Improving upon the works by Arienti [19] and Wescott *et al.* [20], and more recently by Yuan *et al.* [21] on the use of geometric shock dynamics for obtaining the lateral strain rate distribution and failure based on the steady curved detonation theory [22–24] and for predicting the trajectory of the transverse detonation during the re-initiation process of a diffracted cellular detonation wave from a channel, respectively, Radulescu *et al.* [25] extended the critical diffraction criterion using a novel self-similar approximation for the shock dynamics weakly supported by the motion of the detonation products [26]. Apart from the aforementioned (semi-) analytical studies, the curvature-based criterion for critical diffraction condition, i.e., failure due to the curvature of the diffracting detonation greater than a critical value, has also been investigated both numerically and experimentally from other recent studies [27–29] for weakly unstable or stable detonations waves.

Using high-speed flow experimental visualization [18, 30, 31] and numerical simulations [19, 32–34], recent studies revealed more information on the detailed flow features during the diffraction of detonation waves, including the failure dynamics and re-initiation. As evidenced from these studies, the re-initiation is often seen as a consequence of local instabilities at random locations within the region between the lead shock and decoupled reaction zone, forming a local explosion bubble, subsequently leading to the onset of a transverse detonation, which re-initiates the complete diffracting front. At

the critical regime, successful transmission of a diffracting detonation wave thus requires a sufficient degree of cellular instability persisting in the quasi-steady, weakly decoupled reaction-shock complex [31]. This agrees with the current understanding that for unstable mixtures, the initiation and propagation of detonation waves likely have a strong dependence on the transverse waves and cellular instabilities [35, 36]. As previously argued by Lee [37], the failure of an unstable diffracting detonation is closely related to the suppression of cellular instabilities. To elucidate the role played by the cellular instabilities in the critical phenomena of detonation diffraction, Mehrjoo *et al.* [38, 39] and Xu *et al.* [31] experimentally induced artificial flow disturbances using small obstacles at the detonation front. Such effect is also illustrated numerically by Yuan *et al.* [40]. The results obtained by these authors show that the induced instabilities can promote the re-initiation of diffracting unstable detonations.

Quasi-detonations

A quasi-detonation (QD) can be described as a detonation with a velocity noticeably less than the C-J value and an unusual structure [7, 41, 42]. Many studies have investigated QD propagation in obstructed tubes filled with repeated orifice plate obstacles, wherein the dimensions of the orifice diameter and spacing are comparable to the tube diameter [43–51]. In such configurations, the detonation essentially undergoes a series of diffraction and reflection from the obstacles and tube wall as it propagates. The nature of a QD in an obstructed tube, experiencing repeated initiations and failures, may significantly differ from that of an intrinsic cellular detonation propagating in a smooth tube (referred to as an "intrinsic detonation" in the remainder of this paper). The limit phenomena in such configuration is dominated and fostered by losses. Recently, velocity deficits and propagation limits of QDs were investigated in rough-walled tubes [52–55]. The wall roughness was introduced by inserting different wire spirals with diameters comparable to the tube diameter. Unlike a strong obstructing effect imposed by orifice plates, wall roughness introduced by small helical spirals although still generates losses creates also relatively mild perturbations to the structure and underlying dynamics of a QD [56, 57]. Under the influence of these mild perturbations, the degree of the frontal cellular instability could be affected and the turbulent reaction zone of a QD in a rough-walled tube is elongated [7]. Thus, by controlling the artificially introduced wall roughness, one can modify the nature of the cellular instabilities of QDs. This thus per-

mits one to discern the role of the unstable detonation structure competing the effect of losses at near-limit phenomena.

Objective of the current study

The objective of the current study is to further understand the role of cellular instabilities in the critical phenomena—failure and re-initiation processes—of unstable gaseous detonations. To this end, the problem of the critical tube diameter is investigated for QDs generated by rough-walled tubes. This experimental system enables one to vary the extent of detonation instabilities in a relatively controllable manner, and thus, to probe the effect of these instabilities on the detonation failure-vs.-re-initiation mechanisms, with d_c as the metrics. In addition to the experimental effort, this study also consists of a computational analysis to further elucidate qualitatively the nature of QDs and interpret the experimental results. This paper is organized as follows. In Sect. 2, the experimental set-up and the phenomena observed via simultaneous schlieren photography and soot-foil records are first described. The experimental measurement and cell-size scaling of critical tube diameter for quasi-detonation resulting from different wall roughness are then reported and discussed. Section 3 presents the numerical simulations of QD propagation in a two-dimensional representation of rough-walled tubes based on the reactive Euler equations with two-step, induction-reaction chemical kinetics. A more in-depth interpretation of the experimental results inferred by the computational analysis is provided in Sect. 3. The key findings of this study are summarized in Sect. 4.

2. Experiments

2.1. Experimental setup

Figure 1(a) shows a schematic of the experimental setup for this investigation. The experiments were conducted in tubes with inner diameters, D, of 76.2, 50.8, and 25.4 mm, connected to an explosion tank with 25.4 cm inner diameter and 37.5 cm in depth. Two opposed quartz glass windows were installed on both sides of the tank to provide an observational field of view with a 21.54 cm diameter. To generate wall roughness, coil springs of wire diameter (δ) of 2, 3, 6, 7, and 9 mm were used, and the pitch of the springs, L, was maintained at $L = 2\delta$, as shown in the inset of Fig. 1(b). The roughness is defined as the ratio of the wire diameter of the coil to the tube diameter, δ/D. The specific parameters of springs are tabulated in

Table 1. The combustible mixture could be ignited at the left end of the tube by a high-voltage capacitor spark discharge, producing a quasi-steady Chapman-Jouguet (C-J) detonation wave that propagates into the rough-walled section. Equally spaced photo probes were mounted onto the rough section to record the time-of-arrival of the detonation wave. The average velocity between adjacent probes can thus be obtained. A high-speed schlieren system was used to record the process of diffraction and initiation in the explosion tank. The Oriel Apex 200 Watts Hg (Xe) Arc lamp was used as the light source. The maximum frame rate of the high-speed camera (Photron FASTCAM SA1.1) was 30 kfps and the shutter speed was 1/551000 s. The video resolution was 512×352. Note that the detonation outside the exit of the tube, even when it is re-initiated, was not spherical. The velocity was obtained by approximating the wave shape as spherical from the framing schlieren photographs.

In this study, a stoichiometric C_2H_2–O_2 mixture was used as the test gas. The detonation sensitivity of the mixture was controlled by changing the initial pressure (p_0) with a range of 3 to 11 kPa. The initial pressure was monitored by Omega PX309-030AI pressure transducer for high pressure range (0–206 kPa) and PX309-005AI for low pressure (0–34.5 kPa) both with an accuracy of $\pm$ 0.25 % full scale. The digit meter is calibrated to display the minimum pressure reading of 0.01 kPa. The lower pressure range is also checked with a digital manometer model HHP242-015A (0 to 103.4 kPa) with an accuracy of $\pm$ 0.10 % full scale. The mixture was prepared in a separate mixing bottle and allowed to mix for at least 24 hours before each experiment to ensure homogeneity. Note that, owing to the stochastic nature of the near-critical behavior of detonations, it is difficult to unambiguously determine the critical initial pressure, p_c. For each p_0, a set of nine experiments were therefore repeated. The initial pressure was then decremented by 0.1 kPa until no re-initiation can be observed at all.

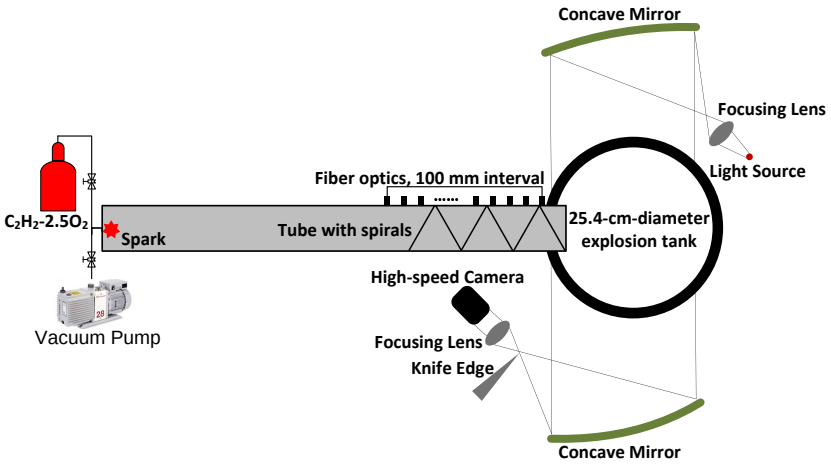

(a)

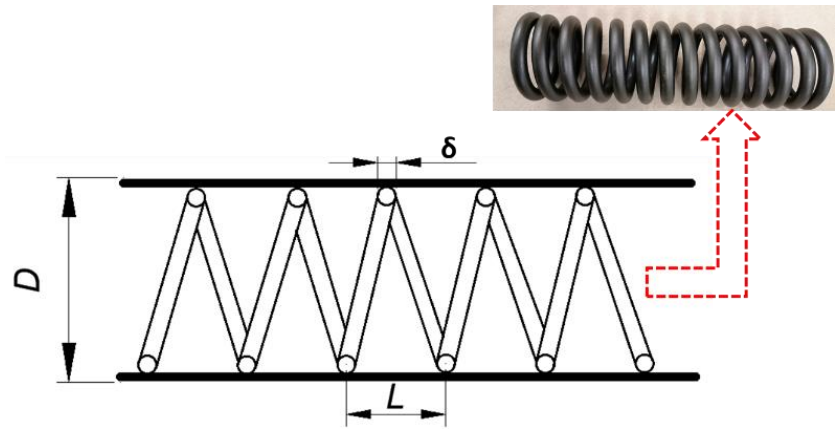

(b)

Figure 1: Schematic of experimental apparatus (a); picture for coil spring (b).

Table 1: sepcific parameters of coil spring

Tube diameter (D) [mm]	Wire Diameter (δ) [mm]	Pitch (L) [mm]	Roughness (δ/D)
25.4	2	4	0.08
	3	6	0.12
50.8	3	6	0.06
	6	12	0.12
76.2	7	14	0.09
	9	18	0.12

2.2. Three transmission modes of detonation diffraction

In the present study, the problem of critical tube diameter for quasi-detonation is investigated systematically in tubes of $D = 25.4$, 50.8, and 76.2 mm. For illustration, Fig. 2 shows some sample schlieren photographs for the 50.8-mm-diameter smooth and rough-walled tubes with various degrees of roughness. The results for tubes of $D = 25.4$ mm and $D = 76.2$ mm are given in the supplementary materials. In all cases, three different propagation modes are observed, i.e., "go", critical, and "no-go" regimes. For the go regime, the emerging detonation from the tube successfully evolves into a spherical detonation. For the no-go case, the detonation fails upon exiting the tube and turns into a deflagration with a diverging shock front decoupled from the reaction zone. For the critical cases, for detonation emerging from both the smooth and rough-walled tubes, the detonation first fails and then is re-initiated from a local explosion center in the reaction zone of the spherical deflagration. The localized explosion centers quickly ignite the shocked, but mostly unreacted, gas behind the decoupled shock front. The triggered reaction waves then spread over the entire diffracting wave front.

Using the frame sequences of the schlieren photos, the velocity of the wave front was determined by locating the wave position and then dividing the distance between two adjacent positions by the time interval. A sample result of the average detonation velocity, $\overline{V}$, normalized by the ideal C-J velocity, V_{CJ}, as a function of initial pressure, p_0, for smooth and rough-walled tubes of $D = 50.8$ mm are shown in Fig. 3. For the go mode, the detonation wave exiting the tube can propagate at the theoretical C-J velocity, V_{CJ}, in the unconfined space. For the no-go mode, the planar detonation exiting from the tube fails eventually, with $\overline{V}$ of the diffracting wave front decreas-

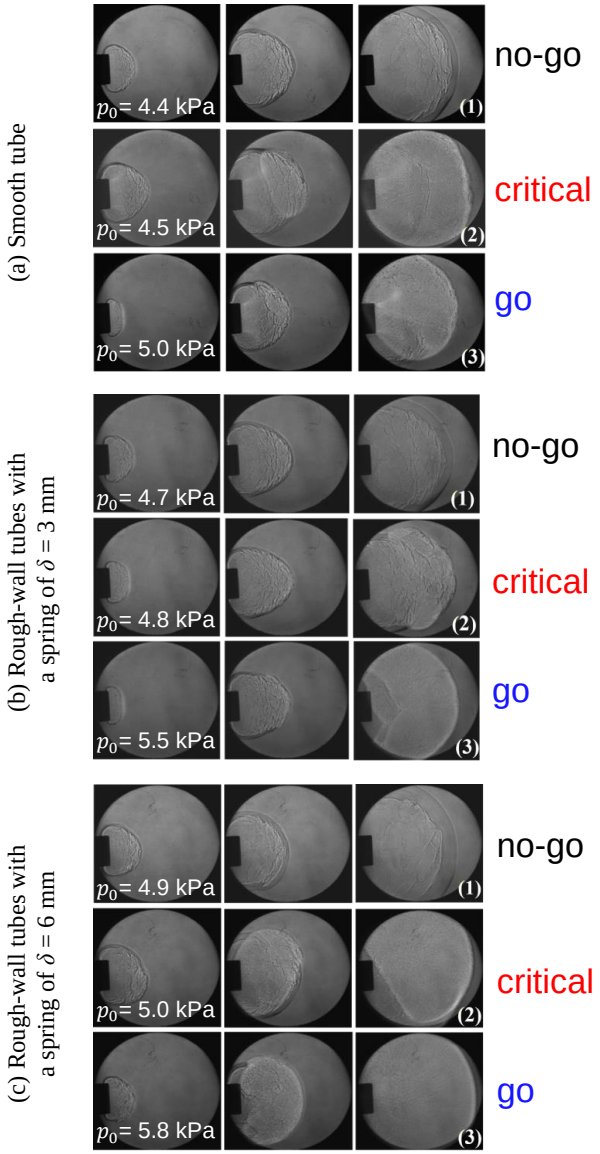

Figure 2: Schlieren photographs for the three propagation modes in 50.8-mm-diameter (a) smooth tube: (1) no-go mode with $p_0 = 4.4\,\text{kPa}$, (2) critical mode with $p_0 = 4.5\,\text{kPa}$, and (3) go mode with $p_0 = 5\,\text{kPa}$; (b) rough-walled tubes with a spring of $\delta = 3\,\text{mm}$: (1) no-go mode with $p_0 = 4.7\,\text{kPa}$, (2) critical mode with $p_0 = 4.8\,\text{kPa}$, and (3) go mode with $p_0 = 5.5\,\text{kPa}$; (c) rough-walled tubes with a spring of $\delta = 6\,\text{mm}$: (1) no-go mode with $p_0 = 4.9\,\text{kPa}$, (2) critical mode with $p_0 = 5.0\,\text{kPa}$, and (3) go mode with $p_0 = 5.8\,\text{kPa}$.

ing to approximately $0.2V_{\mathrm{CJ}}$. For the critical regime, the average velocity fluctuates between 0.2 and $0.9V_{\mathrm{CJ}}$. It is difficult to unambiguously determine a unique critical pressure p_{c}. For the repeated experiments at each p_0, only if successful re-initiation is observed in all of the repeated experiments, the case with the corresponding p_0 is considered as a go mode. Similarly, only if all of the repeated experiments result in a failure of re-initiation, the case is considered as a no-go mode. The critical regime, wherein re-initiation is observed in some of the repeated experiments, lies over a range of p_0 between the go and no-go modes. As shown in Fig. 3, the ranges of critical pressure indicated by the purple dashed lines are 4.5-4.9 kPa, 4.8-5.0 kPa, and 5.0-5.5 kPa in 50.8-mm-diameter smooth tube and rough-walled tubes with $\delta = 3$ mm and $\delta = 6$ mm springs, respectively.

The local velocity of the wave front, V, normalized by V_{CJ}, as a function of distance from the initiation point (i.e., the spark discharge), is plotted in Fig. 4 for cases with the 50.8-mm diameter smooth tube and rough-walled tubes filled with $\delta/D = 0.06$ and 0.12. In each plot, the first data point is obtained at $x = 170$ mm where the spring-filled section starts for the rough-walled cases. The vertical dashed line indicates the location of the tube exit. Results for other tube diameters are provided in the supplementary materials. In the rough-walled tubes, the QD propagates at a velocity significantly lower than the C-J value as shown in Fig. 5, i.e., the normalized average propagation velocity of QDs, $\overline{V}/V_{\mathrm{CJ}}$, plotted as a function of p_0. In Fig. 4, three diffraction modes can be identified. For the "go" mode, the propagation velocity is nearly unaffected by the diffraction in the unconfined space. For the "no-go" mode, the local wave velocity decreases from approximately $V/V_{\mathrm{CJ}} = 0.9$ to 0.2 after exiting the tube, and the detonation eventually fails to propagate. For the critical regime, large fluctuations, ranging from $V/V_{\mathrm{CJ}} = 0.2$ to 0.9, in local propagation velocity, are observed in the unconfined space.

To summarize, Fig. 6 presents the range of critical (initial) pressure, p_{c}, as a function of wall roughness, δ/D, for the cases with tubes of $D = 25.4$ mm, 50.8 mm, and 76.2 mm. Zero roughness refers to the smooth tube case. Each data point represents the average value of p_{c} of the nine measurements for the specific tube diameter and roughness. The error bar indicates the range of p_0 corresponding to the critical mode as identified in Fig. 3. It can be seen that, for all of the tube diameters, the average critical pressure shows only

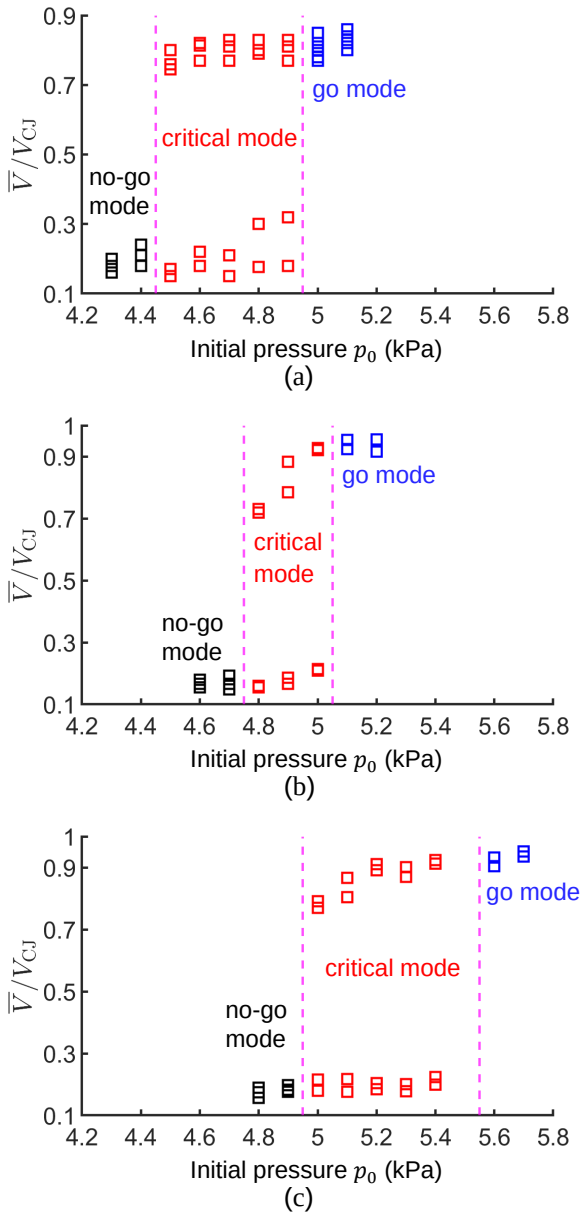

Figure 3: Average propagation velocity of the wave front, $\overline{V}$, normalized by the ideal C-J speed, plotted as a function of initial pressure, p_0, in the unconfined space after exiting from (a) a smooth tube and rough-walled tubes with springs of (b) $\delta/D = 0.06$ and (c) $\delta/D = 0.12$. The inner diameter of the tubes is $D = 50.8\,\mathrm{mm}$.

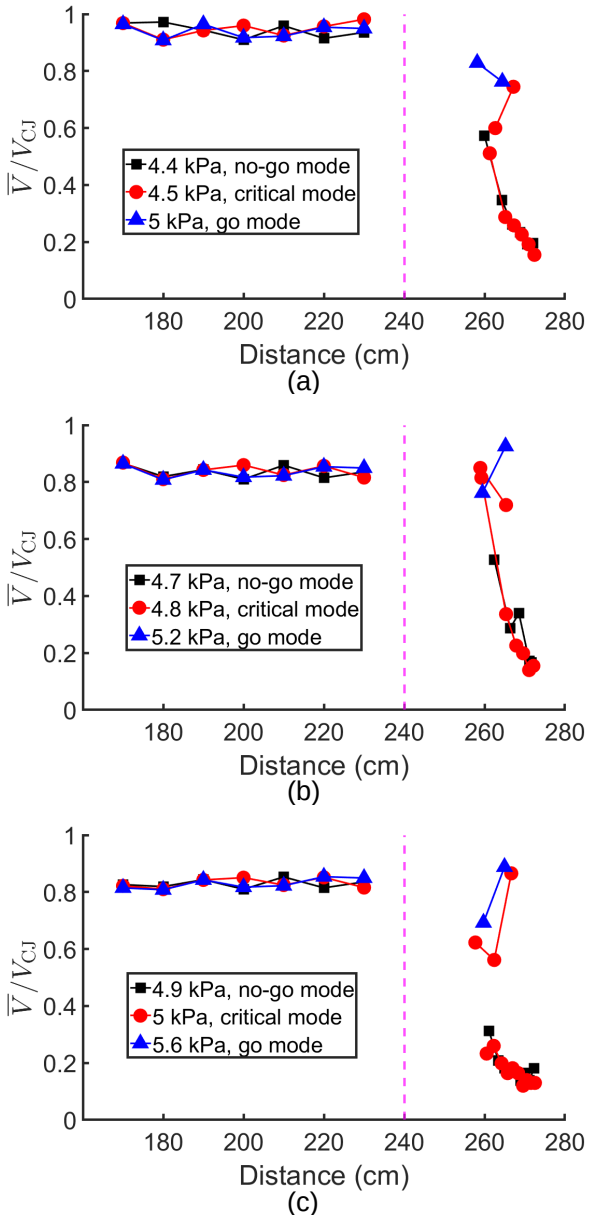

Figure 4: Local propagation velocity of the wave front, V, normalized by the ideal C-J speed, plotted as a function of distance measured from the initiation point (i.e., the spark discharge) for the cases with (a) a smooth tube and rough-walled tubes with springs of (b) $\delta/D = 0.06$ and (c) $\delta/D = 0.12$. The vertical dashed line indicates the location of the tube exit. The inner diameter of the tubes is $D = 50.8\,\mathrm{mm}$.

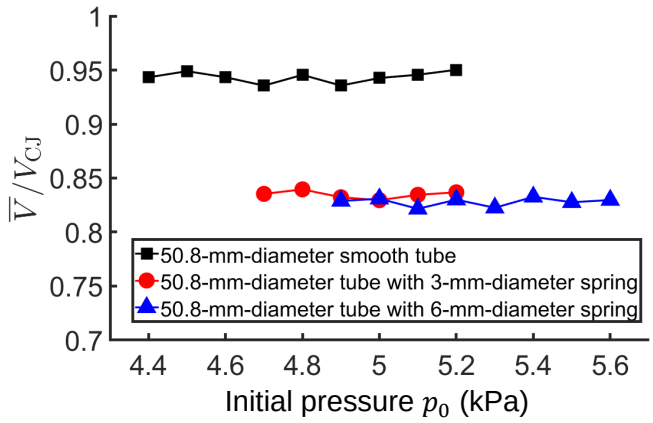

Figure 5: Average propagation velocity inside the tube, $\overline{V}$, normalized by the ideal C-J speed, plotted as a function of initial pressure, p_0, for the cases with a smooth tube (black squares) and rough-walled tubes with springs of $\delta/D = 0.06$ (red circles) and $\delta/D = 0.12$ (blue triangles). The inner diameter of the tubes is $D = 50.8\,\text{mm}$.

a negligible increase in rough tubes compared with the corresponding value for the intrinsic cellular detonation (resulting from a smooth tube) at the same diameter. Compared to the losses and the level of velocity deficits due to the roughness and the reduction in the see-through diameter, this slight increase in pressure (i.e., less than 0.5 kPa) is minimal and not significant, even considering the error bars.

2.3. Critical regime of detonation diffraction

The cell sizes for QDs in rough tubes were measured using the standard smoked-foil technique. The typical cellular patterns are presented in Fig. 7. As in [52–55], the foil was inserted into the inner diameter of the spiral and hence, it records only the cellular structure of the detonation core. Although the smoked foil shields the detonation from the roughness at the wall, it is found that the detonation structure is refrained for some distance of travel after entering the smoked foil section. Thus, the foil can still capture the detonation structure in the rough tube. The data of cell size are plotted as a function of initial pressure for the tubes with different diameters and roughnesses in Fig. 8. The relationship between λ and p_0 is approximately linear. At the same p_0, the cell size for quasi-detonations in rough tubes is larger than the intrinsic cell size resulting from a smooth tube. In addition,

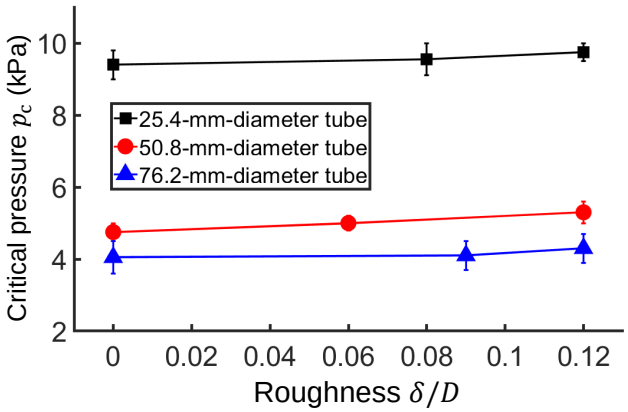

Figure 6: Critical pressure as a function of roughness (δ/D).

to quantify the critical regime of detonation initiation, the scaling of d_c/λ is considered at the critical initial pressure. In this study, to account for the presence of wall roughness, the physical scale of the tube is characterized by the see-through diameter $d_c = D - 2\delta$, where D is tube diameter and δ is the spiral spring diameter [52]. Thus, d_c represents the central core diameter of the rough tube. A non-dimensional ratio of physical scale d_c to chemical scale λ is therefore used in order to further illustrate the critical condition for the detonation diffraction.

The experimental results of d_c/λ for both intrinsic detonations and QDs are presented in Table 2. The ratio is determined using the cell size values determined in the present study for both smooth and rough walled tubes. In smooth tubes without coil springs, the critical condition is consistent with the previous scaling ratio of $d_c/\lambda \approx 13$. For QDs in rough-walled tubes, the scaling ratio significantly deviates from 13. Based on the results of this study, the critical initiation condition for QD can be quantified as $d_c/\lambda \approx 8$, indicating that the number of detonation cells required for a successful transmission of a QD into an unconfined space less than that for an intrinsic detonation. Certainly, the smaller ratio can be due to the reduction of the see-through diameter with roughness and also the enlargement of detonation cells in the rough tube. In fact, even determining this ratio using cell sizes measured from smooth tubes for each corresponding critical pressure (with very slight difference), the similar decreasing trend for QDs in rough-walled

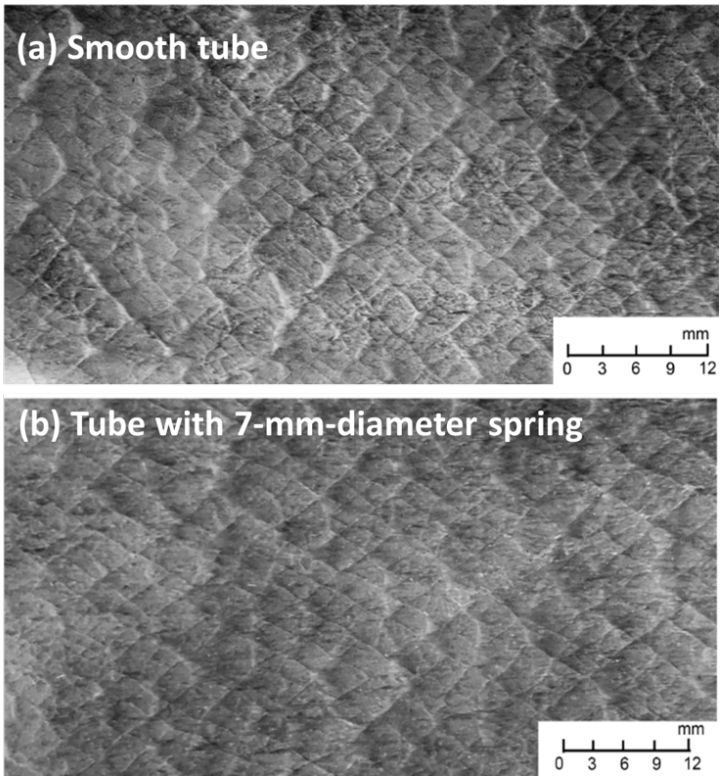

Figure 7: Typical cellular structures for p_0= 4 kPa in 76.2-mm-diameter tube, (a) smooth tube; (b) tube with 7-mm-diameter spring.

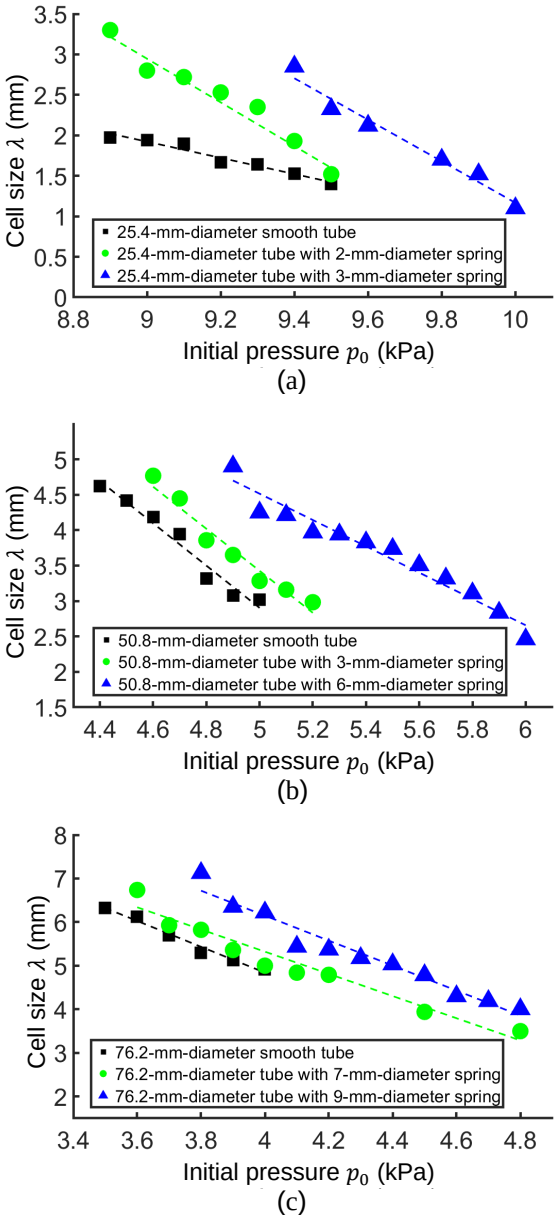

Figure 8: Cell size as a function of initial pressure in tube with different diameters: (a) $D = 25.4\,\text{mm}$, (b) $D = 50.8\,\text{mm}$, and (c) $D = 76.2\,\text{mm}$. The dotted line represents the curve fit.

Table 2: Experimental results for critical tube diameter

Tube diameter (D) [mm]	Tube type	p_c [kPa]	λ [mm]	d_c [mm]	d_c/λ [mm]
25.4	smooth	9	1.94	25.4	13.09
	rough-wall $\delta = 2\,$mm	9.1	2.72	21.4	7.87
	rough-wall $\delta = 3\,$mm	9.5	2.33	19.4	8.33
50.8	smooth	4.5	4.42	50.8	11.49
	rough-wall $\delta = 3\,$mm	4.8	3.86	44.8	11.61
	rough-wall $\delta = 6\,$mm	5	4.25	38.8	9.13
76.2	smooth	3.6	6.12	76.2	12.45
	rough-wall $\delta = 7\,$mm	3.7	5.93	62.6	10.49
	rough-wall $\delta = 9\,$mm	3.9	6.35	58.2	9.17

tubes is also obtained (i.e., d_c/λ decreases with increasing roughness). Using the cell size correlation [58] obtained from data tabulated in [59] and [60], as well the limited data measured in this study for the smooth tube, the following correlations can be obtained, respectively:

$$\lambda\,[\text{mm}] = 28.7 \cdot (p_o)[\text{kPa}]^{-1.26} \tag{1}$$

$$\lambda\,[\text{mm}] = 31.30412 \cdot (p_o)[\text{kPa}]^{-1.283217} \tag{2}$$

and Table 3 shows d_c/λ scaling using cell sizes determined from the above two correlations.

The rather negligible increase in critical pressure for quasi-detonation, as shown in Fig. 6, can still be attributed to a lower propagation velocity prior to exiting the tube. It is, however, of interest to remark that this increase in p_c is slight despite the fact that the average detonation velocity decreases much more significantly, i.e., approximately from $\overline{V}/V_{CJ} = 0.95$ to 0.8, for an increasingly greater wall roughness. In addition to the losses introduced by the rough wall, mild perturbations are also generated to the propagating detonation front without destroying its overall cellular characteristics. These seemingly contradicting results suggest that the transmission capability of a cellular detonation into an unconfined space is not only governed by the average velocity (or strength) of the incident detonation, but also the nature of cellular instabilities. To more clearly elucidate the difference in the nature of cellular instabilities between an intrinsic detonation in a smooth tube and a QD in a rough-walled tube, an explanatory modeling effort is made in this study.

Table 3: Scaling for the critical conditions using cell size values measured in smooth tube

Tube diameter (D) [mm]	Tube type	p_c [kPa]	d_c/λ (using Eq.1) [mm]	d_c/λ (using Eq.2) [mm]
25.4	smooth	9	14.10	13.61
	rough-wall $\delta = 2\,\text{mm}$	9.1	12.05	11.63
	rough-wall $\delta = 3\,\text{mm}$	9.5	11.53	11.14
50.8	smooth	4.5	11.78	11.18
	rough-wall $\delta = 3\,\text{mm}$	4.8	11.27	10.71
	rough-wall $\delta = 6\,\text{mm}$	5	10.27	9.78
76.2	smooth	3.6	13.34	12.59
	rough-wall $\delta = 7\,\text{mm}$	3.7	11.34	10.71
	rough-wall $\delta = 9\,\text{mm}$	3.9	11.27	10.66

3. Explanatory model via numerical simulations

3.1. Model description and numerical methodologies

A computational analysis is performed to illustrate how rough-walled-induced QDs differ from an intrinsic, unstable cellular detonation in a smooth tube. Since this analysis aims to qualitatively capture the essential features of QDs, a reactive-flow paradigm based on the inviscid Euler equations with simplified chemical kinetics, i.e., a two-step, induction-reaction model [40, 61], is used. All the parameters have been non-dimensionalized with respect to the uniform, unburned state ahead of the detonation front. With the two-step kinetic model, the one-dimensional ZND induction zone length (Δ_I) is employed as the reference unit length, i.e., $\Delta_\text{I} = 1$. The solutions to the governing equations are obtained numerically using a second-order MUSCL-Hancock scheme with an HLLC (Harten-Lax-van Leer-Contact) approximate Riemann solver [62, 63] with a CFL (Courant–Friedrichs–Lewy) number of 0.90. The simulations are accelerated by GPU-enabled parallel computing [63, 64]. In this study, the normalized thermodynamic parameters of the combustible mixture are fit into the two-step method, approximately representing a stoichiometric hydrogen-oxygen mixture at 20 kPa and 300 K [40]. Using the cell size and critical tube data from the CALTECH Detonation Database [59], we can obtain the following correlation for the stoichiometric hydrogen-oxygen mixture at different initial pressure:

$$\lambda\,[\text{mm}] = 181.42 \cdot (p_o)[\text{kPa}]^{-1.0417} \tag{3}$$

$$d_{\mathrm{c}}\,[\mathrm{mm}] = 2075.4 \cdot (p_o)[\mathrm{kPa}]^{-0.99763} \tag{4}$$

For an initial pressure range of 5 kPa to 25 kPa, it can be shown that the critical tube diameter follows the universal scaling: $d_{\mathrm{c}} \approx 12.28$ to 13.18λ, respectively. Thus, hydrogen-oxygen mixtures at the given conditions follow the same scaling and hence, exhibit qualitatively similar dynamic behavior of unstable detonations.

In order to represent a three-dimensional rough tube as a two-dimensional channel, as shown in Fig. 9, the spring coils are approximated as staggered square obstacles along the top and bottom boundaries of the computational domain. An incident detonation wave with a fully developed cellular structure is initially placed near the left end of the domain and propagates rightward into the rough-walled section. To obtain a quasi-steady detonation wave in the rough channel, a sufficiently long propagation distance is required. An advancing-window technique, following the method proposed by Li *et al.* [65, 66] in the literature of detonation modeling, is used in this study to reduce the use of data memory and computational time for simulating detonation waves propagating over a long distance. Two grid resolutions of 10 and 20 computational cells per the ZND induction-zone length, i.e., $\Delta_{\mathrm{I}}/\Delta x = 10$ and 20, respectively, are selected for the herein reported simulations. The grid resolution study is previously reported in [40]. The recent study by Shi *et al.* [34] using one-step Arrhenius kinetics also shows a similar resolution level, i.e., a 16 pts per half-reaction zone length $\Delta_{1/2}$ is deemed sufficient to determine critical conditions and 24 pts/$\Delta_{1/2}$ for high-precision examination of the structure. The computational domain is a 600×300 rectangle so that the channel width D is 300 times of Δ_{I}. As indicated in Fig. 9, the size of each square obstacle is denoted as δ. The length between two consecutive obstacles, L, is fixed as $L = 4\delta$.

3.2. Simulation results and statistical analysis

The density fields and numerical soot foils obtained with a computational resolution of $\Delta_{\mathrm{I}}/\Delta x = 20$ for the smooth channel and rough-walled channels with $\delta/D = 0.05$ and 0.1 are presented in Fig. 10. Noticeably, the cellular detonation structure is strongly affected by the roughness. The cellular patterns become more irregular for the cases with an increasingly greater wall roughness. As shown in Fig. 10(c), i.e., the rough-walled case with $\delta/D = 0.1$, the cellular pattern almost vanishes in some regions while relatively fine cells are formed in some other regions. The cell sizes of QD are significantly greater

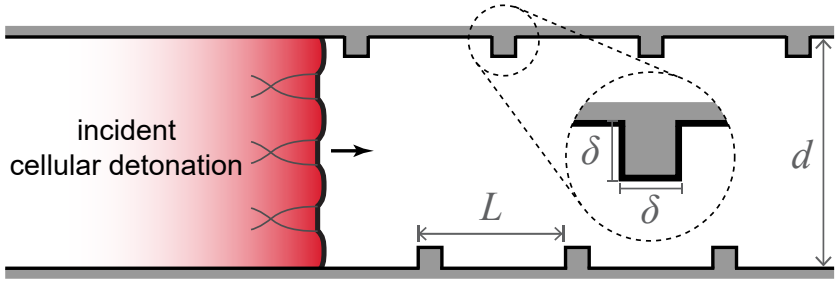

Figure 9: Schematic showing the domain configuration for the simulation of a detonation wave propagating in a rough-walled channel.

than those resulting from a smooth channel. This finding is consistent with the experimental measurements reported in Fig. 8.

The induction-reaction-zone dynamics of an intrinsic cellular detonation resulting from a smooth channel and QDs in rough-walled channels are further scrutinized via a statistical analysis. With the present two-step kinetic model [61], the induction rate $\dot{\omega}_{\mathrm{I}}$ is expressed as follows,

$$\dot{\omega}_{\mathrm{I}} = \rho k_{\mathrm{I}} \exp\left[E_{\mathrm{I}}\left(\frac{1}{T_{\mathrm{s}}} - \frac{1}{T}\right)\right] \tag{5}$$

where T_{S} is the post-shock temperature, E_{I} the activation energy, and k_{I} the pre-exponential rate constant of induction. As illustrated in Fig. 11(a), the simulation data of $\dot{\omega}_{\mathrm{I}}$ is collected in a window following a non-planar pattern of the detonation front. This data-collection window has a width of 20 and 60 times Δ_{I} ahead and behind the shock front, respectively. The top and bottom boundaries of the data window are aligned with the inner surface of the obstacles. In order to reduce the noise introduced by the transient fluctuations of an unstable detonation, data were collected from 200 flow-field snapshots over a period of 1000 units of time. During this time, the detonation propagates over a distance of 5300 times Δ_{I}, i.e., about 9 times the channel width.

Figure 11(b) presents the probability density function (p.d.f.) of the induction rate behind the wave front obtained with a resolution of $\Delta_{\mathrm{I}}/\Delta x = 20$. For the cases with smooth and rough-walled channels, the distribution peaks at different values. The overall distribution and the peak values are moving leftwards with an increase in wall roughness. To quantify the spread of the

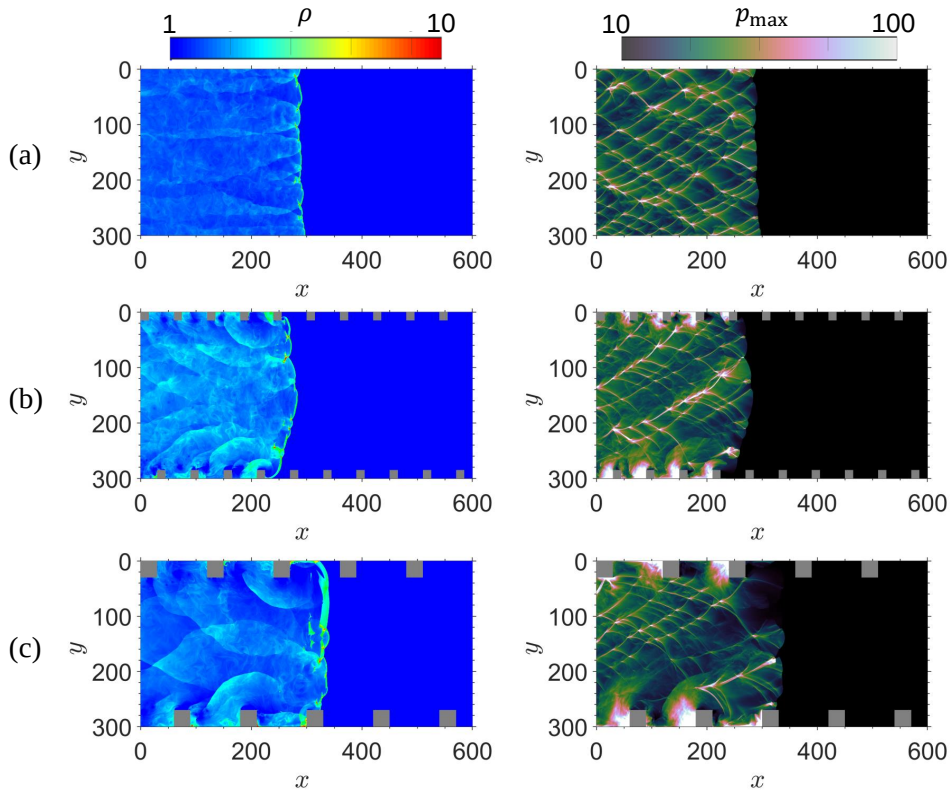

Figure 10: The density field and soot foils in a 300×600 computational domain for the cases with (a) a smooth channel and rough-walled channels of (b) $\delta/D = 0.05$ and (c) $\delta/D = 0.1$.

p.d.f. curves of $\dot{\omega}_{\mathrm{I}}$, the standard deviation, σ, is calculated.

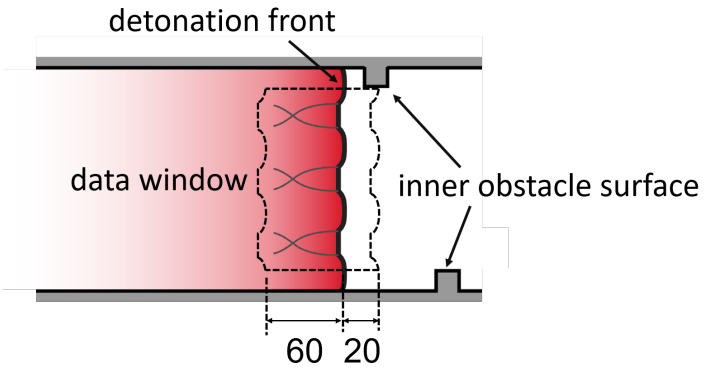

(a)

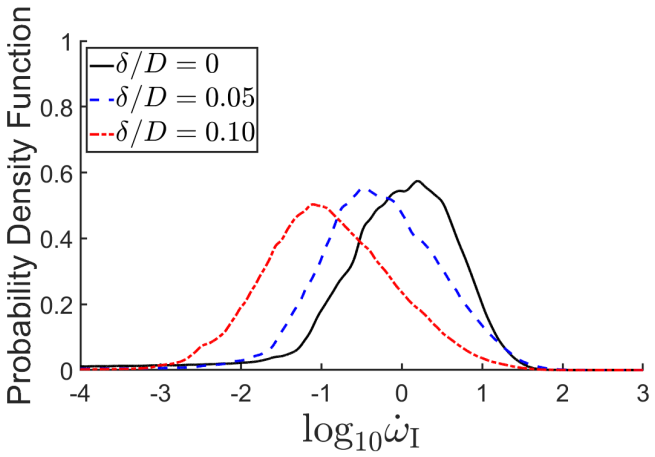

(b)

Figure 11: (a) Schematic of the data window around the detonation front and (b) the probability density function of induction rate at the resolution of $\Delta_{\mathrm{I}}/\Delta x = 20$.

Figure 12 shows the standard deviation of the p.d.f. of $\dot{\omega}_{\mathrm{I}}$ (right axis) and the average detonation velocity normalized by the C-J speed (left axis) as functions of wall roughness, δ/D, obtained from simulations at two different grid resolutions, i.e., $\Delta_{\mathrm{I}}/\Delta x = 10$ and 20. The cellular patterns in smooth tube (i.e., $\delta/D = 0$) obtained with these two grid resolutions are also provided for comparison. The results plotted in Fig. 12 demonstrate that σ increases and $\overline{V}/V_{\mathrm{CJ}}$ decreases monotonically as wall roughness increases. The leftward shifting of the p.d.f. curve towards smaller $\dot{\omega}_{\mathrm{I}}$ (as shown in Fig. 11(b)) is due to the decrease in average detonation velocity in an in-

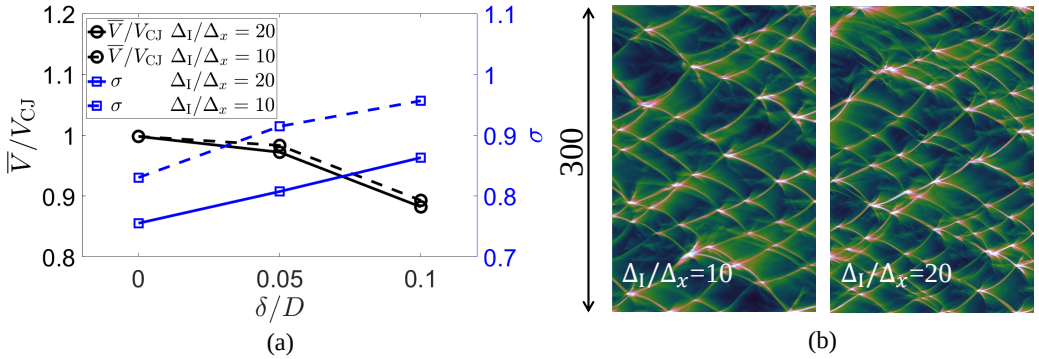

Figure 12: (a) The average detonation velocity normalized by the C-J detonation velocity $\overline{V}/V_{\mathrm{CJ}}$ (black circles, left axis) and the standard deviation σ of the probability distribution of induction rate (blue squares, right axis) as functions of wall roughness, δ/D, and (b) the numerical soot foil showing the cellular structures. The results are obtained from simulations at two different grid resolutions, i.e., $\Delta_{\mathrm{I}}/\Delta x = 10$ and 20.

creasingly rougher channel, as shown in Fig 12. An increase in σ indicates that the spread of the probability distribution of $\dot{\omega}_{\mathrm{I}}$ becomes wider as wall roughness increases. These results suggest that, although the bulk induction-reaction rates of a QD are reduced by the obstacles, the instabilities induced by the wall roughness broaden the probability distribution of the induction-reaction rates of a QD. In the critical-tube-diameter problem, therefore, this extension towards faster induction-reaction rates may compensate the effect of a reduced propagation speed of a QD on its transmission capability into an unconfined space. The key finding of this computational analysis is independent of grid resolution as the trends of $\overline{V}/V_{\mathrm{CJ}}$ and σ with δ/D remain unchanged for both low- and high-resolution simulations as shown in Fig. 12.

To further investigate the propagation dynamics of a QD, transient simulation results are analyzed. Figure 13 shows the oscillation of the transient, spatially averaged (over the y-direction) induction-zone length, $\bar{l}_{\mathrm{ind}}$, for the case with $\delta/D = 0.1$. The large fluctuations in $\bar{l}_{\mathrm{ind}}$ can be seen in Fig. 13. As shown in Fig. 13(a), a local peak of $\bar{l}_{\mathrm{ind}}$ is associated with the moment when the shock front is decoupled with the reaction zone, and the cellular structure fades away. A local minimum of $\bar{l}_{\mathrm{ind}}$ occurs at the moment when the QD has a fully developed cellular structure with a reaction zone closely attached to the shock front as shown in Fig. 13(b).

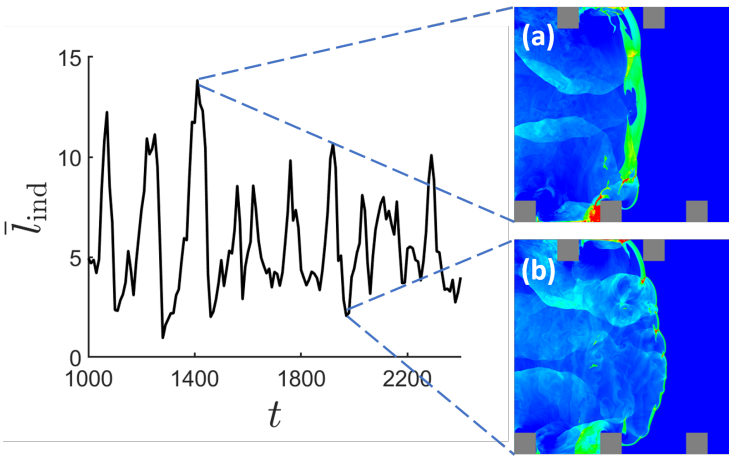

Figure 13: The time-dependent spatial average induction zone length ($\bar{l}_{\mathrm{ind}}$) distribution when $\delta/D = 0.1$: (a) the density contour showing that the detonation front is decoupling and the cellular structure is fading away with high $\bar{l}_{\mathrm{ind}}$, (b) the density contour showing the cellular detonation structure with low $\bar{l}_{\mathrm{ind}}$.

Figure 14 shows a sample of a numerical smoked foil for a QD propagating in a rough-walled channel. The spatial distribution of the cellular pattern is highly irregular as seen in smoked foil. There exist regions of re-initiation at overdriven state giving birth to small detonation cells and local quenching leaving behind unburnt shock reactive pockets (Fig. 15). Among these temporary local decoupling regions, the induction rate is much lower than that occurring at the shock front of the corresponding steady C-J detonation. Thus, the propagation of a QD is a series of repeated partly quenching induced by the obstacles and re-initiation triggered by strong local explosions.

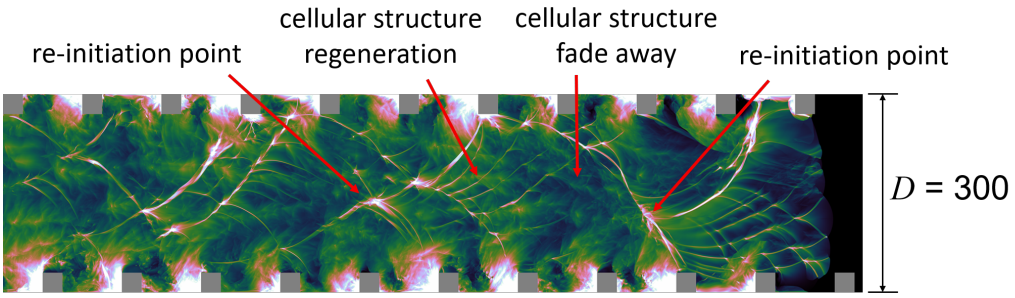

Figure 14: The soot foil showing the periodical cellular dynamics of a quasi-detonation propagating in a rough channel with $\delta/D = 0.1$.

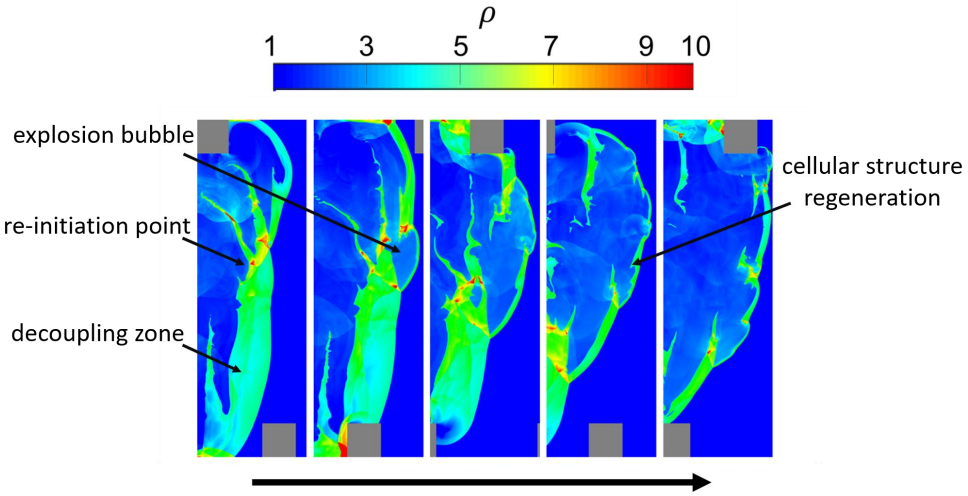

Figure 15: Density contours in a series of transient frames showing the unstable features and the re-initiation process at the quasi-detonation front.

4. Concluding remarks

In the present study, the propagation and diffraction of quasi-detonation using stoichiometric acetylene-oxygen mixtures in three different diameter tubes with different spiral inserts to generate roughness have been examined via experiments. Two-dimensional numerical simulations using a simplified model have also been conducted to complement qualitatively the present experimental finding. The motivation behind this work is to elucidate how the unstable detonation structure influences the critical tube diameter. Besides the losses introduced by the rough wall, mild perturbations are also generated to the propagating detonation front without destroying its overall cellular characteristics. Despite the velocity deficit due to losses in rough tubes, the experimental results only show a negligible change in the critical pressure for the critical tube diameter. It is hypothesized that the negative effect of velocity losses is compensated by the resulting perturbations and additional instabilities to the cellular detonation structure, i.e., stronger local hot spots produced by the more turbulent structure and instability for quasi-detonation.

For the critical tube diameter of quasi-detonation, the conventional $d_c/\lambda \geq 13$ criterion appears invalid, and the critical regime for quasi-detonation can be quantified approximately as $d_c/\lambda \approx 8$ where the cell size λ corresponds the value measured in the rough tube. The even lower critical value again indicates the importance of increasing instabilities, i.e., the more unstable fluctuations before exiting from the tube for quasi-detonation, which provides a favorable effect on the detonation transmission by inducing stronger local hot spots.

The propagation dynamics of quasi-detonation in rough tubes are also illustrated through the two-dimensional numerical simulations. In agreement with the experimental measurement, the cell sizes, in general, are greater for quasi-detonation in rough tubes than that for normal cellular detonation. A more "turbulent" flow structure for quasi-detonation is also observed numerically with a larger variational spectrum of induction rate despite the cell size enlargement. From the present study, the characteristics of the detonation frontal structure can once again be confirmed to play a crucial role in determining the dynamic detonation parameters. The effect of multi-dimensional instabilities on the critical tube diameter for quasi-detonations will be further explored numerically in future work.

Acknowledgements

This research is supported by the China Scholarship Council (CSC), the Natural Sciences and Engineering Research Council of Canada (NSERC) and the National Key R&D Program of China (No. 2021YFB4000902). The authors thank A.J. Higgins for useful feedback on the manuscript.

References

[1] Y. B. Zel'dovich, An experimental investigation of spherical detonation of gases, Soviet Phys. Tech. Phys. 1 (1956) 1689–1713.

[2] V. V. Mitrofanov, R. I. Soloukhin, The diffraction of multi-front detonation waves, Sov. Phys. Dokl. 9 (12) (1965) 1055–1058.

[3] J. H. S. Lee, Dynamic parameters of gaseous detonations, Annu. Rev. Fluid Mech. 16 (1984) 311–336.

[4] A. A. Vasil'ev, Dynamic parameters of detonations, Shock Waves Science and Technology Library, Vol 6: Detonation Dynamics, edited by F. Zhang. Chap. 4, Springer-Verlag, Berlin, Heidelberg, 2012.

[5] K. Kailasanath, Recent developments in the research on pulse detonation engines, AIAA J. 41 (2) (2003) 145–159.

[6] G. D. Roy, S. M. Frolov, A. A. Borisov, D. W. Netzer, Pulse detonation propulsion: challenges, current status, and future perspective, Progr. Energy Combust. Sci. 30 (2004) 545–672.

[7] J. H. S. Lee, The Detonation Phenomenon, Cambridge University Press, Cambridge, 2008.

[8] H. Matsui, J. H. S. Lee, On the measure of the relative detonation hazards of gaseous fuel-oxygen and air mixtures, Proc. Combust. Inst. 17 (1979) 1269–1280.

[9] R. Knystautas, J. H. S. Lee, C. Guirao, The critical tube diameter for detonation failure in hydrocarbon-air mixtures, Combust. Flame 48 (1982) 63–83.

[10] I. Sochet, T. Lamy, J. Brossard, C. Vaglio, R. Cayzac, Critical tube diameter for detonation transmission and critical initiation energy of spherical detonation, Shock Waves 9 (1999) 113–123.

[11] B. Zhang, H. D. Ng, J. H. S. Lee, Measurement and relationship between critical tube diameter and critical energy for direct blast initiation of gaseous detonations, J. Loss Prev. Proc. Ind. 26 (2013) 1293–1299.

[12] D. Desbordes, C. Guerraud, L. Hamada, H. N. Presles, Failure of classical dynamic parameters relationships in highly regular cellular detonation systems, Prog. Astronaut. Aeronaut. 153 (1993) 347–359.

[13] I. Moen, A. Sulmistras, G. O. Thomas, D. Bjerketvedt, P. A. Thibault, Influence of cellular regularity on the behavior of gaseous detonations, Prog. Astronaut. Aeronaut. 106 (1983) 220–243.

[14] B. Zhang, N. Mehrjoo, H. D. Ng, J. H. S. Lee, C. H. Bai, On the dynamic detonation parameters in acetylene-oxygen mixtures with varying amount of argon dilution, Combust. Flame 161 (5) (2014) 1390–1397.

[15] Y. Nagura, J. Kasahara, Y. Sugiyama, A. Matsuo, Comprehensive visualization of detonation diffraction structures and sizes in unstable and stable mixtures, Proc. Combust. Inst. 34 (2013) 1949–1956.

[16] A. Kawasaki, J. Kasahara, A novel characteristic length of detonation relevant to supercritical diffraction, Shock Waves 30 (2020) 1–12.

[17] C. A. Eckett, J. J. Quirk, J. E. Shepherd, The role of unsteadiness in direct initiation of gaseous detonations, J. Fluid Mech. 421 (2000) 147–183.

[18] F. Pintgen, J. E. Shepherd, Detonation diffraction in gases, Combust. Flame 156 (3) (2009) 665–677.

[19] M. Arienti, J. Shepherd, A numerical study of detonation diffraction, J. Fluid Mech. 529 (2005) 117–146.

[20] B. L. Wescott, D. S. Stewart, J. B. Bdzil, On self-similarity of detonation diffraction, Phys. Fluids 16 (2004) 373–384.

[21] X. Q. Yuan, X. C. Mi, H. D. Ng, J. Zhou, A model for the trajectory of the transverse detonation resulting from re-initiation of a diffracted detonation, Shock Waves 30 (2020) 13–15.

[22] L. T. He, P. Clavin, On the direct initiation of gaseous detonations by an energy source, J. Fluid Mech. 277 (1994) 227–248.

[23] J. Yao, D. S. Stewart, On the normal detonation shock velocity - curvature relationship for materials with large activation energy, Combust. Flame 100 (1995) 519–528.

[24] R. Klein, J. C. Krok, J. E. Shepherd, Curved quasi-steady detonations: Asymptotic analysis and detailed chemical kinetics, Tech. Rep. California Institute of Technology, Pasadena, California (1995) GALCIT Report FM 95–04.

[25] M. I. Radulescu, R. Mével, Q. Xiao, S. Gallier, On the self-similarity of diffracting gaseous detonations and the critical channel width problem, Phys. Fluids 33 (2021) 066106.

[26] M. I. Radulescu, On the shock change equations, Phys. Fluids 32 (2020) 056106.

[27] J. Meredith, H. D. Ng, J. H. S. Lee, Detonation diffraction from an annular channel, Shock Waves 20 (6) (2010) 449–455.

[28] J. Li, J. Ning, C. B. Kiyanda, H. D. Ng, Numerical simulation of cellular detonations diffraction in stable gaseous mixtures, Propul. Power Res. 5 (3) (2016) 177–183.

[29] R. Mevel, Q. Xiao, M. I. Radulescu, Hydrogen-oxygen- argon detonation diffraction in a narrow channel, in: Proceedings of the 26th International Colloquium on Dynamics of Explosions and Reactive Systems, Boston, MA, 2017.

[30] F. P. Pintgen, Detonation diffraction in mixtures with various degrees of instability, Dissertation (Ph.D.), California Institute of Technology, CA, USA (2005).

[31] H. Xu, X. C. Mi, C. B. Kiyanda, H. D. Ng, J. H. S. Lee, The role of cellular instability on the critical tube diameter problem for unstable gaseous detonations, Proc. Combust. Inst. 37 (3) (2019) 3545–3553.

[32] D. A. Jones, G. Kemister, N. Tonello, E. Oran, M. Sichel, Numerical simulation of detonation reignition in H_2–O_2 mixtures in area expansions, Shock Waves 10 (2000) 33–41.

[33] S. Gallier, F. Le-Palud, F. Pintgen, R. Mével, J. E. Shepherd, Detonation wave diffraction in H_2–O_2–Ar mixtures, Proc. Combust. Inst. 36 (2017) 2781–2789.

[34] L. Shi, K. C. K. Uy, C. Y. Wen, The re-initiation mechanism of detonation diffraction in a weakly unstable gaseous mixture, J. Fluid Mech. 895 (2020) A24.

[35] F. Pintgen, C. A. Eckett, J. M. Austin, J. E. Shepherd, Direct observations of reaction zone structure in propagating detonations, Combust. Flame 133 (3) (2003) 211–229.

[36] M. I. Radulescu, J. H. S. Lee, The failure mechanism of gaseous detonations: experiments in porous wall tubes, Combust. Flame 131 (1-2) (2002) 29–46.

[37] J. H. S. Lee, On the critical tube diameter. In: Bowen, J. (ed.) Dynamics of Exothermicity, p. 321., Gordon and Breach, Amsterdam, 1996.

[38] N. Mehrjoo, B. Zhang, R. Portaro, H. D. Ng, J. H. S. Lee, Response of critical tube diameter phenomenon to small perturbations for gaseous detonations, Shock Waves 24 (2) (2014) 219–229.

[39] N. Mehrjoo, Y. Gao, C. B. Kiyanda, H. D. Ng, J. H. S. Lee, Effects of porous walled tubes on detonation transmission into unconfined space, Proc. Combust. Inst. 35 (2) (2015) 1981–1987.

[40] X. Q. Yuan, C. Yan, J. Zhou, H. D. Ng, Computational study of gaseous cellular detonation diffraction and re-initiation by small obstacle induced perturbations, Phys. Fluids 33 (2021) 047115.

[41] G. Ciccarelli, S. Dorofeev, Flame acceleration and transition to detonation in a duct, Prog. Energy Comb. Sci. 34 (2008) 449–550.

[42] B. E. Gelfand, M. V. Silnikov, S. P. Medvedev, S. V. Khomik, Fast deflagration and quasi-detonation, Thermo-Gas Dynamics of Hydrogen Combustion and Explosion, Springer, Berlin, Heidelberg, 2012.

[43] A. Teodorczyk, J. H. S. Lee, R. Knystautas, Propagation mechanism of quasi-detonations, Proc. Combust. Inst. 22 (1988) 1723–1731.

[44] A. Teodorczyk, J. H. S. Lee, R. Knystautas, Photographic study of the structure and propagation mechanisms of quasi-detonations in rough tubes, AIAA Prog. Astronaut. Aeronaut. 133 (1991) 223–240.

[45] G. Ciccarelli, M. Cross, On the propagation mechanism of a detonation wave in a round tube with orifice plates, Shock Waves 26 (5) (2016) 587–597.

[46] G. Ciccarelli, Z. Wang, J. Lu, M. Cross, Effect of orifice plate spacing on detonation propagation, J. Loss Prev. Process Ind. 49 (2017) 739–744.

[47] B. Zhang, L. Hong, The effects of large scale perturbation-generating obstacles on the propagation of detonation filled with methane-oxygen mixture, Combust. Flame 182 (2017) 279–287.

[48] L. Q. Wang, H. H. Ma, Z. W. Shen, M. J. Lin, X. J. Li, Experimental study of detonation propagation in a square tube filled with orifice plates, Int. J. Hydrogen Energy 43 (9) (2018) 4645–4656.

[49] L. Q. Wang, H. H. Ma, Z. W. Shen, Effect of orifice plates on detonation propagation in stoichiometric hydrogen-oxygen mixture, Exp. Thermal Fluid Sci. 99 (2018) 367–373.

[50] G. Rainsford, D. J. S. Aulakh, G. Ciccarelli, Visualization of detonation propagation in a round tube equipped with repeating orifice plates, Combust. Flame 198 (2018) 205–211.

[51] M. Kellenberger, G. Ciccarelli, Three-dimensional behavior of quasi-detonation, Combust. Flame 215 (2020) 145–156.

[52] A. Starr, J. H. S. Lee, H. D. Ng, Detonation limits in rough walled tubes, Proc. Combust. Inst. 35 (2) (2015) 1989–1996.

[53] B. Zhang, The influence of wall roughness on detonation limits in hydrogen–oxygen mixture, Combust. Flame 169 (2016) 333–339.

[54] T. Ren, Y. Yan, H. Zhao, J. H. S. Lee, H. D. Ng, Propagation of near-limit gaseous detonations in rough-walled tubes, Shock Waves 30 (2020) 769–780.

[55] Y. Liu, J. H. S. Lee, H. Tan, H. D. Ng, Investigation of near-limit detonation propagation in a tube with helical spiral, Fuel 286 (2) (2021) 119384.

[56] H. Guénoche, The detonation and deflagration of gas mixtures, Rev. Inst. Français Pétrole 4 (1949) 48–69.

[57] N. Manson, C. Brochet, J. Brossard, Y. Pujol, Vibratory phenomena and instability of self-sustained detonations in gases, Proc. Combust. Inst. 9 (1963) 461–469.

[58] B. Zhang, N. Mehrjoo, H. D. Ng, J. H. S. Lee, C. Bai, On the dynamic detonation parameters in acetylene-oxygen mixtures with varying amount of argon dilution, Combust. Flame 161(5) (2014) 1390–1397.

[59] M. Kaneshige, J. E. Shepherd, Detonation database, Technical Report FM97-8, GALCIT, July 1997 (https://shepherd.caltech.edu/detndb/html/db.html).

[60] M. I. Radulescu, The propagation and failure mechanism of gaseous detonations: experiments in porous-walled tubes, Dissertation (Ph.D.), McGill University, QC, Canada (2003).

[61] H. D. Ng, M. I. Radulescu, A. J. Higgins, N. Nikiforakis, J. H. S. Lee, Numerical investigation of the instability for one-dimensional chapman–jouguet detonations with chain-branching kinetics, Combust. Theor. Model. 9 (3) (2005) 385–401.

[62] E. F. Toro, Riemann Solvers and Numerical Methods for Fluid Dynamics, Springer, Berlin, Heidelberg, 2019.

[63] C. B. Kiyanda, G. H. Morgan, N. Nikiforakis, H. D. Ng, High resolution gpu-based flow simulation of the gaseous methane-oxygen detonation structure, J. Vis. 18 (2) (2015) 273–276.

[64] X. C. Mi, A. J. Higgins, H. D. Ng, C. B. Kiyanda, N. Nikiforakis, Propagation of gaseous detonation waves in a spatially inhomogeneous reactive medium, Phys. Rev. Fluids 2 (5) (2017) 053201.

[65] J. Li, X. Mi, A. Higgins, Effect of spatial heterogeneity on near-limit propagation of a pressure-dependent detonation, Proc. Combust. Inst. 35 (2015) 2025–2032.

[66] J. Li, X. Mi, A. J. Higgins, Geometric scaling for a detonation wave governed by a pressure-dependent reaction rate and yielding confinement, Phys. Fluids 27 (2015) 027102.